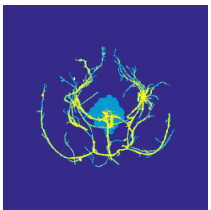
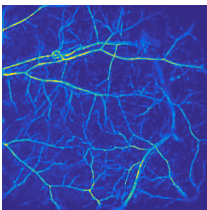
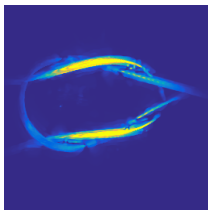


Variational Image Reconstruction in 4D Photoacoustic Tomography



Felix Lucka

University College London

f.lucka@ulc.ac.uk

joint with:

Simon Arridge, Paul Beard,
Marta Betcke, Ben Cox,
Nam Huynh & Edward Zhang



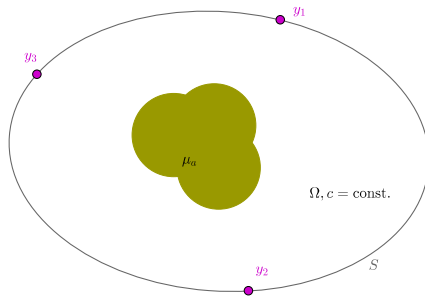
Centre for Medical Image Computing

Manchester, November 12, 2015.

Optical Part

optical absorption coefficient: μ_a

Acoustic Part

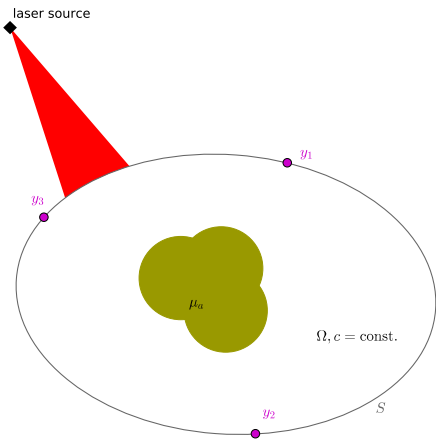


Optical Part

optical absorption coefficient: μ_a

pulsed laser excitation: Φ

Acoustic Part



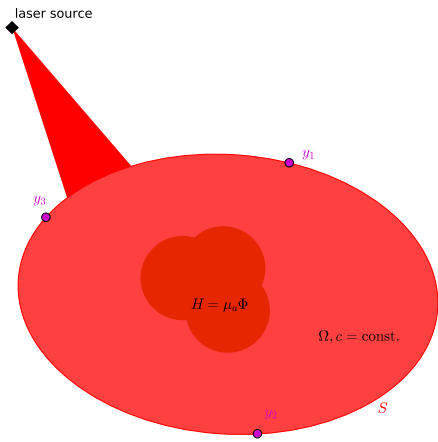
Optical Part

optical absorption coefficient: μ_a

pulsed laser excitation: Φ

thermalization by chromophores: $H = \mu_a \Phi$

Acoustic Part



Optical Part

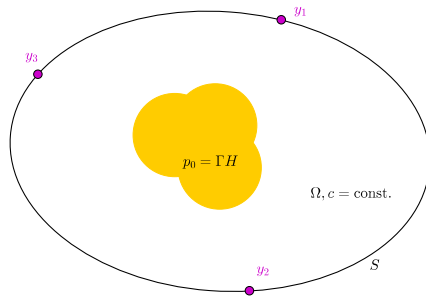
optical absorption coefficient: μ_a

pulsed laser excitation: Φ

thermalization by chromophores: $H = \mu_a \Phi$

Acoustic Part

local pressure increase: $p_0 = \Gamma H$



Optical Part

optical absorption coefficient: μ_a

pulsed laser excitation: Φ

thermalization by chromophores: $H = \mu_a \Phi$

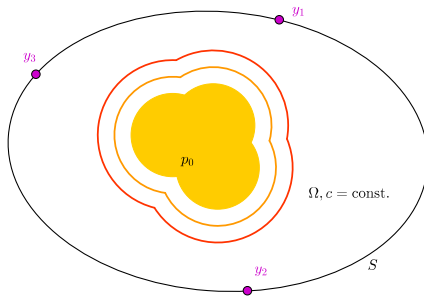
Acoustic Part

local pressure increase: $p_0 = \Gamma H$

elastic wave propagation:

$$\Delta p - \frac{1}{c^2} \frac{\partial^2 p}{\partial^2 t} = 0$$

$$p|_{t=0} = p_0, \quad \frac{\partial p}{\partial t}|_{t=0} = 0$$



Optical Part

optical absorption coefficient: μ_a

pulsed laser excitation: Φ

thermalization by chromophores: $H = \mu_a \Phi$

Acoustic Part

local pressure increase: $p_0 = \Gamma H$

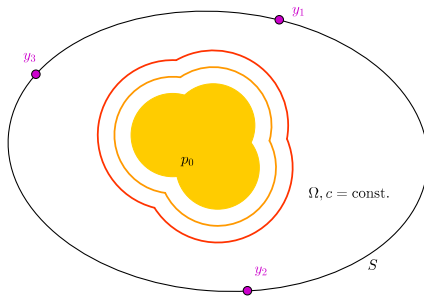
elastic wave propagation:

$$\Delta p - \frac{1}{c^2} \frac{\partial^2 p}{\partial t^2} = 0$$

$$p|_{t=0} = p_0, \quad \frac{\partial p}{\partial t}|_{t=0} = 0$$

measurement of pressure time courses:

$$f_i(t) = p(y_i, t)$$



Optical Part

optical absorption coefficient: μ_a

pulsed laser excitation: Φ

thermalization by chromophores: $H = \mu_a \Phi$

Acoustic Part

local pressure increase: $p_0 = \Gamma H$

elastic wave propagation:

$$\Delta p - \frac{1}{c^2} \frac{\partial^2 p}{\partial^2 t} = 0$$

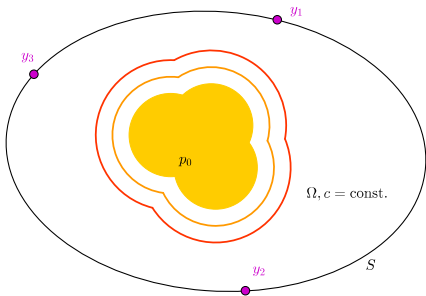
$$p|_{t=0} = p_0, \quad \frac{\partial p}{\partial t}|_{t=0} = 0$$

measurement of pressure time courses:

$$f_i(t) = p(y_i, t)$$

Photoacoustic effect

- ▶ coupling of optical and acoustic modalities.
- ▶ "hybrid imaging"
- ▶ high optical contrast can be read by high-resolution ultrasound.



Optical Part

optical absorption coefficient: μ_a

pulsed laser excitation: Φ

thermalization by chromophores: $H = \mu_a \Phi$

Acoustic Part

local pressure increase: $p_0 = \Gamma H$

elastic wave propagation:

$$\Delta p - \frac{1}{c^2} \frac{\partial^2 p}{\partial^2 t} = 0$$

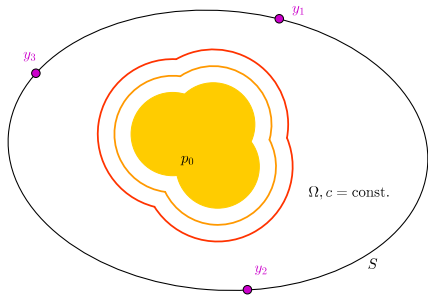
$$p|_{t=0} = p_0, \quad \frac{\partial p}{\partial t}|_{t=0} = 0$$

measurement of pressure time courses:

$$f_i(t) = p(y_i, t)$$

Inverse problems:

! optical inversion (μ_a) from boundary data: **severely ill-posed**.



Optical Part

optical absorption coefficient: μ_a

pulsed laser excitation: Φ

thermalization by chromophores: $H = \mu_a \Phi$

Acoustic Part

local pressure increase: $p_0 = \Gamma H$

elastic wave propagation:

$$\Delta p - \frac{1}{c^2} \frac{\partial^2 p}{\partial t^2} = 0$$

$$p|_{t=0} = p_0, \quad \frac{\partial p}{\partial t}|_{t=0} = 0$$

measurement of pressure time courses:

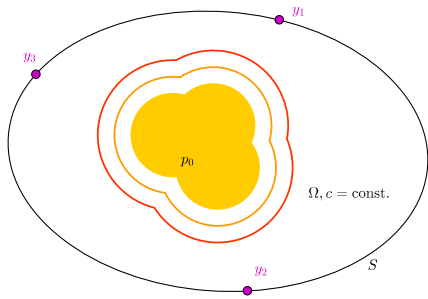
$$f_i(t) = p(y_i, t)$$

Inverse problems:

! optical inversion (μ_a) from boundary data: **severely ill-posed**.

✓ acoustic inversion (p_0) from boundary data: **moderately ill-posed**.

✓ optical inversion (μ_a) from **internal** data: **moderately ill-posed**.



Optical Part

optical absorption coefficient: μ_a

pulsed laser excitation: Φ

thermalization by chromophores: $H = \mu_a \Phi$

Acoustic Part

local pressure increase: $p_0 = \Gamma H$

elastic wave propagation:

$$\Delta p - \frac{1}{c^2} \frac{\partial^2 p}{\partial t^2} = 0$$

$$p|_{t=0} = p_0, \quad \frac{\partial p}{\partial t}|_{t=0} = 0$$

measurement of pressure time courses:

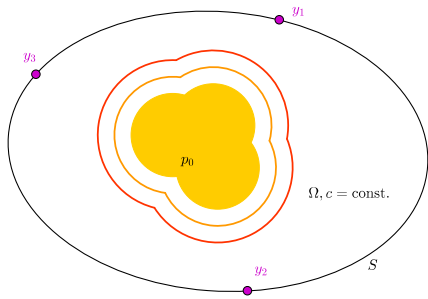
$$f_i(t) = p(y_i, t)$$

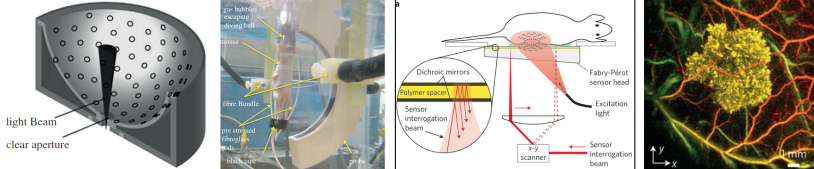
Inverse problems:

! optical inversion (μ_a) from boundary data: severely ill-posed.

✓ acoustic inversion (p_0) from boundary data: moderately ill-posed.

✓ optical inversion (μ_a) from internal data: moderately ill-posed.





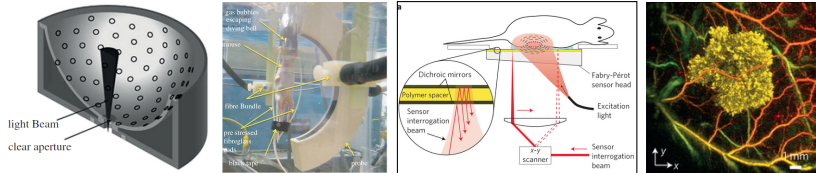
from: Beard, 2011, *Interface Focus*; Jathoul et al., 2015, *Nature Photonics*

Piezoelectric arrays:

- ! low spatial resolution
- ✓ high temporal resolution
- ! moderate sensitivity
- ✓ flexible wrt geometry

Fabry-Pérot interferometer:

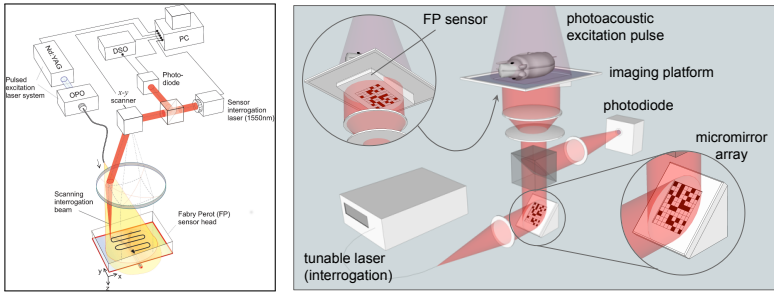
- ✓ high spatial resolution
- ! low temporal resolution
- ✓ high sensitivity
- ! only planar geometries.



from: Beard, 2011, *Interface Focus*; Jathoul et al., 2015, *Nature Photonics*

Aim of our project

Increase dynamic frame rate of FB-PAT by combining advances in spatio-temporal sub-sampling/compressed sensing and inverse problems with the development of tailored data acquisition systems.



- ▶ Single-point sub-sampling (structured or random).
- ▶ Patterned interrogation by micromirror array, similar to "[single-pixel](#)" Rice camera.
- ▶ Multi-beam scanning + sub-sampling.

Huynh et al., 2014. *Patterned interrogation scheme for compressed sensing photoacoustic imaging using a Fabry Perot planar sensor,* Proc. SPIE 8943.

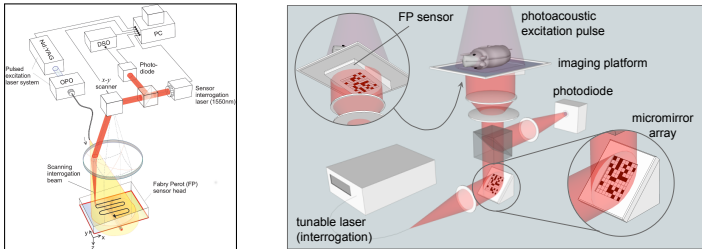


Image model:

$$f_i^c = G_i f_i = G_i (A p_i + \varepsilon_i)$$

for each frame i .

Image reconstruction:

- ▶ $f_i^c \rightarrow f_i$, $f_i \rightarrow p_i$ by standard method, frame-by-frame.
- ▶ $f_i^c \rightarrow p_i$: standard or new method, frame-by-frame.
- ▶ $F^c \rightarrow F$, $f_i \rightarrow p_i$ by standard method, frame-by-frame.
- ▶ $F^c \rightarrow P$: Full spatio-temporal method.

Analytic methods, e.g. eigenfunction expansion and closed-form filtered-backprojection, are too restrictive for us.

Time Reversal (TR):

- ▶ "Least restrictive PAT reconstruction"
- ▶ Sending the recorded waves "back" into volume.
- ▶ Requires a numerical model for acoustic wave propagation.

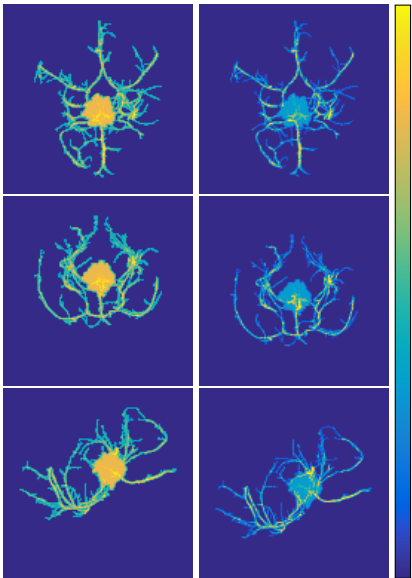
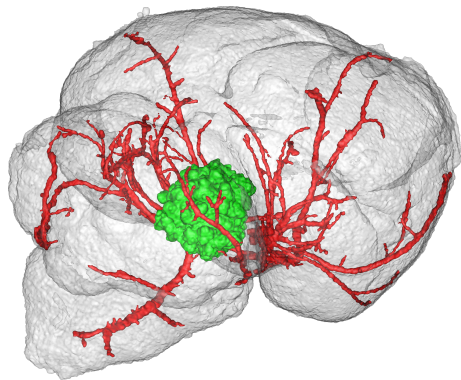
k-Wave^(*) implements a *k*-space pseudospectral method to solve the underlying system of first order conservation laws:

- ▶ Compute spatial derivatives in Fourier space: 3D FFTs.
- ▶ Modify finite temporal differences by *k*-space operator and use staggered grids for accuracy and robustness.
- ▶ Perfectly matched layer to simulate free-space propagation.
- ▶ Parallel/GPU computing leads to massive speed-ups.

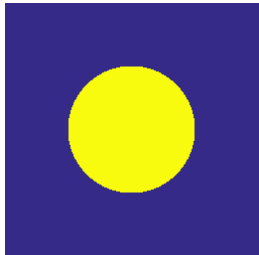


(*) B. Treeby and B. Cox, 2010. k-Wave: MATLAB toolbox for the simulation and reconstruction of photoacoustic wave fields, *Journal of Biomedical Optics*.

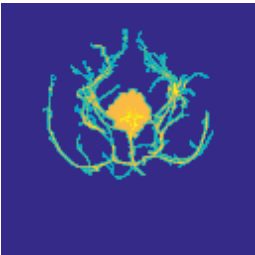
A Realistic Numerical Phantom



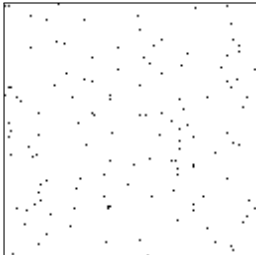
Time Reversal for Sub-Sampled Data



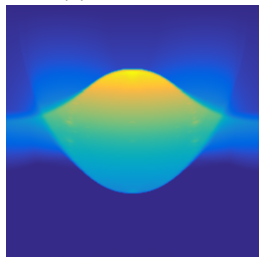
(a) IC, $n = 256^3$



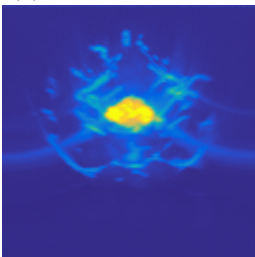
(b) high con., IC, $n = 128^3$



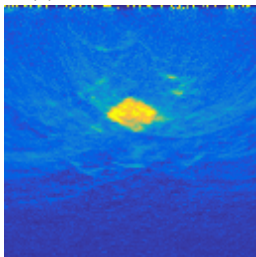
(c) sub-sampling, 1/128



(d) TR 1



(e) TR 2



(f) TR 2, sub-sampled

planar sensor on top; **inverse crime data**; maximum intensity projections, side view

Solving variational regularization problems

$$\hat{p}_i = \operatorname{argmin}_{p \geq 0} \left\{ \frac{1}{2} \|G_i A p - f_i^c\|_2^2 + \lambda \mathcal{J}(p) \right\}$$

by first-order methods requires numerical representation of A and A^* .

k-Wave yields a discrete representation A_κ^{dis} . For A^* , one can

1) adjoint k-Wave iteration to obtain $(A_\kappa^{dis})^*$:

- ✓ high numerical accuracy.
- ! tedious derivation, specific for k-Wave, limited insights.

Huang, Wang, Nie, Wang, Anastasio, 2013. *IEEE Trans Med Imaging*

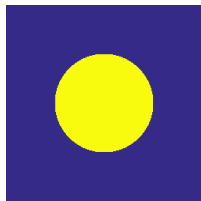
2) derive analytical adjoint and discretize it, e.g., $(A^*)_\kappa^{dis}$.

- ✓ sufficient numerical accuracy.
- ✓ theoretical insights, generalizes to all numerical schemes.

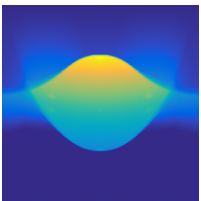
Arridge, Beard, Betcke, Cox, Huynh, L, Zhang, 2015. *On the Adjoint Operator in Photoacoustic Tomography, (in preparation for PMB)*.

Comparison for Full Data

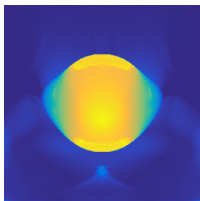
$$\hat{p}_i = \underset{p \geq 0}{\operatorname{argmin}} \left\{ \frac{1}{2} \|Ap - f\|_2^2 + \lambda \mathcal{J}(p) \right\}$$



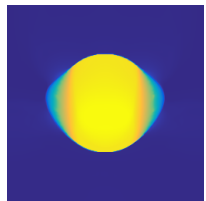
(a) $n = 256^3$



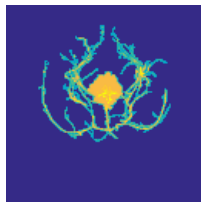
(b) TR



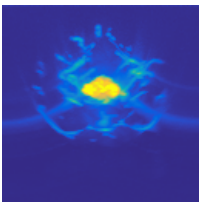
(c) LS⁺



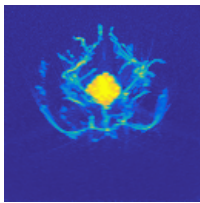
(d) TV⁺



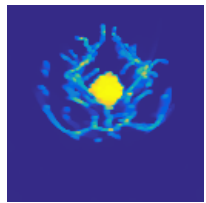
(e) high con., $n = 128^3$



(f) TR

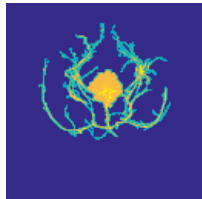


(g) LS⁺

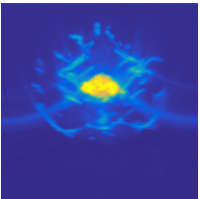


(h) TV⁺, Breg

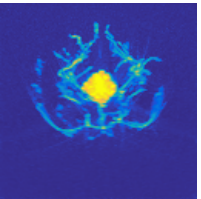
planar sensor on top; **inverse crime data**; maximum intensity projections, side view



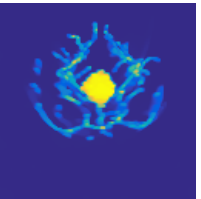
(a) Phantom



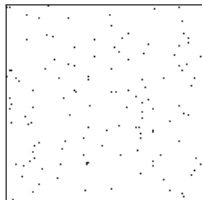
(b) TR



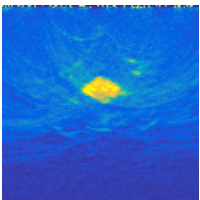
(c) LS⁺



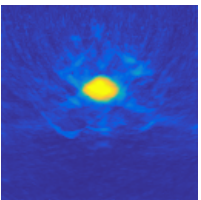
(d) TV⁺, Breg



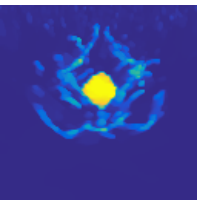
(e) Sub, 1/128



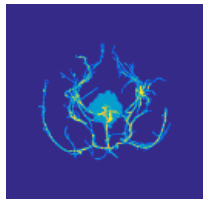
(f) TR



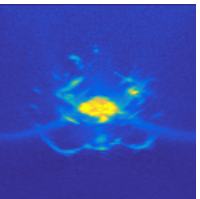
(g) LS⁺



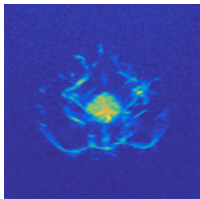
(h) TV⁺, Breg



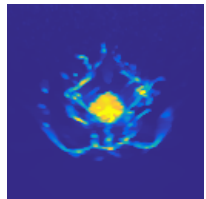
(a) Phantom



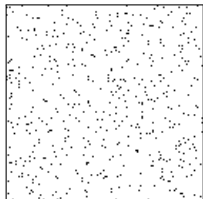
(b) TR



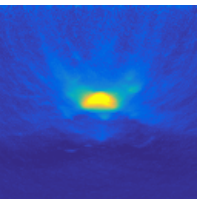
(c) LS^+



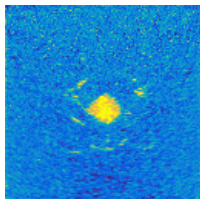
(d) TV^+



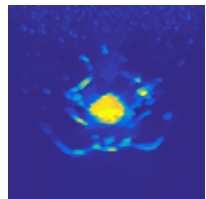
(e) Sub, 1/32



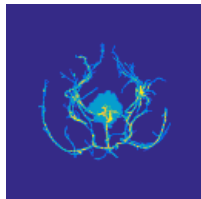
(f) TR



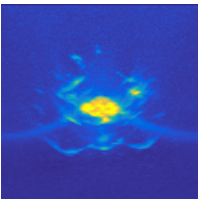
(g) LS^+



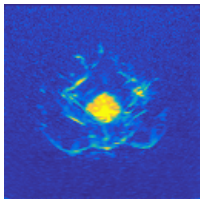
(h) TV^+



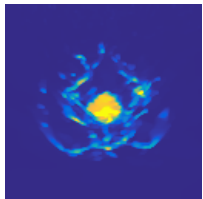
(a) Phantom



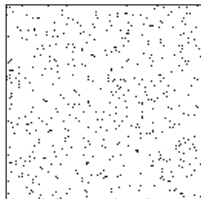
(b) TR



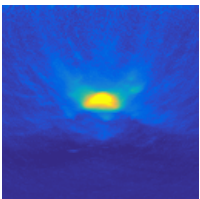
(c) LS^+



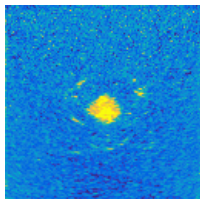
(d) TV^+



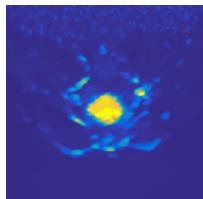
(e) Sub, 1/32



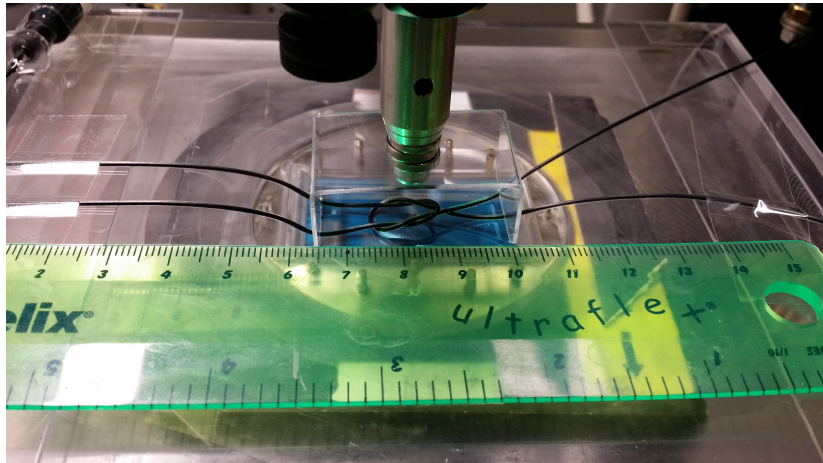
(f) TR



(g) LS^+



(h) TV^+



- ▶ Two polythene tubes filled with 10/100% ink.
- ▶ Stop-motion-style data acquisition of pulling one tube end.
- ▶ 45 frames (15min acquisition time per frame).
- ▶ Full data reconstructions to validate sub-sampling.

Full Data: Good Ground Truth?



Time Reversal

TV^+

full data

sub-sampling

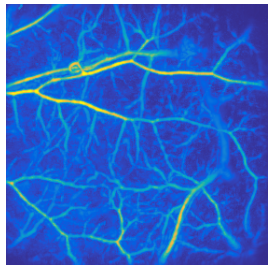
full data

sub-sampling

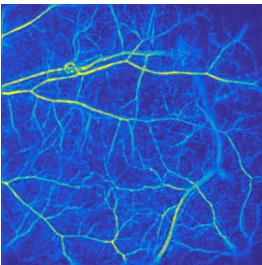
full data

sub-sampling

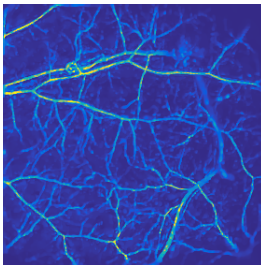
In Vivo Measurements: Full Data



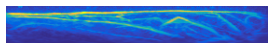
(a) TR, x



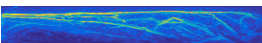
(b) PI+, x



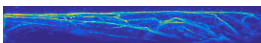
(c) TV+, x



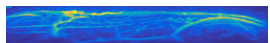
(d) TR, y



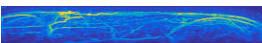
(e) PI+, y



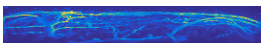
(f) TV+, y



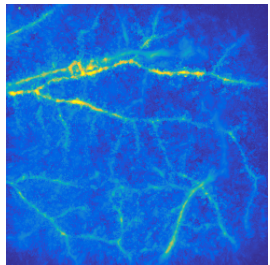
(g) TR, z



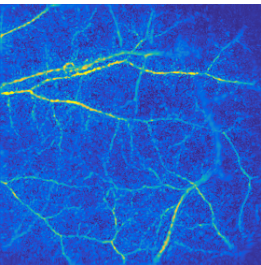
(h) PI+, z



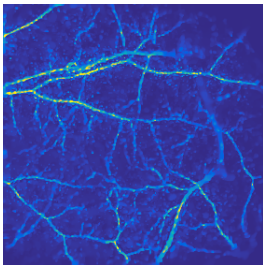
(i) TV+, z



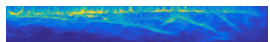
(a) TR, x



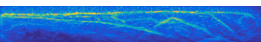
(b) PI+, x



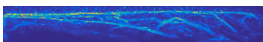
(c) TV+, x



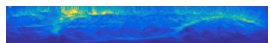
(d) TR, y



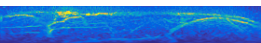
(e) PI+, y



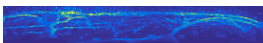
(f) TV+, y



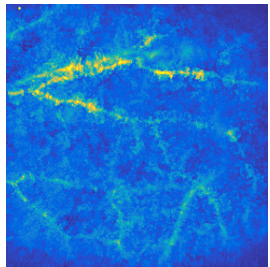
(g) TR, z



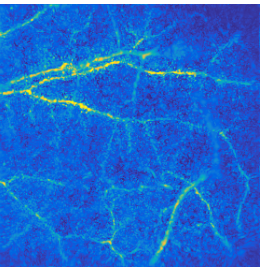
(h) PI+, z



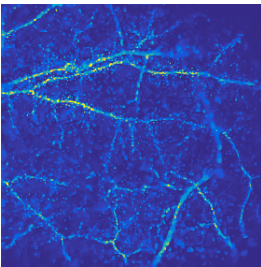
(i) TV+, z



(a) TR, x



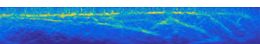
(b) PI+, x



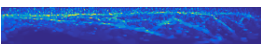
(c) TV+, x



(d) TR, y



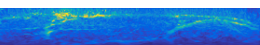
(e) PI+, y



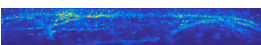
(f) TV+, y



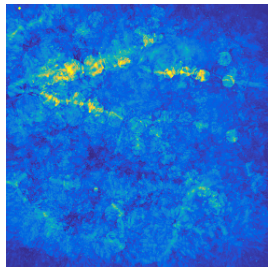
(g) TR, z



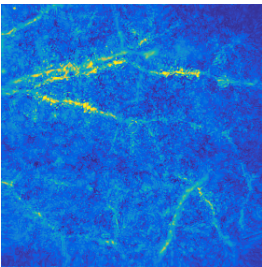
(h) PI+, z



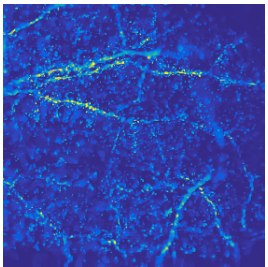
(i) TV+, z



(a) TR, x



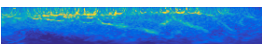
(b) PI+, x



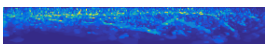
(c) TV+, x



(d) TR, y



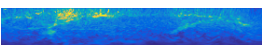
(e) PI+, y



(f) TV+, y



(g) TR, z



(h) PI+, z



(i) TV+, z

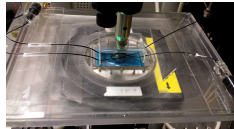
A strong sub-sampling requires:

- ▶ Accurate model fit:
 - ! inhomogeneous optical excitation
 - ! uncertainty of acoustic parameters
 - ! inhomogeneity and defects of FB sensor
 - ! data artifacts by reflections / external sources

Not all of these defects can be simulated in a meaningful way.

- ⇒ Develop suitable, automatic pre-processing.
- ⇒ Refine forward model used.
- ⇒ Refine no-inverse-crime simulations.

- ▶ Suitable regularization functionals:
 - ! TV is limited, especially for in-vivo data.
 - ! Experimental phantoms and in-vivo data are different.
- ⇒ Develop suitable regularizing functionals.



Continuous data acquisition

⇒ tradeoff between spatial and temporal resolution.

Different dynamic models:

- ▶ Low-Rank (functional imaging with static anatomies).
- ▶ Low-Rank + sparsity.
- ▶ Tracer uptake models.
- ▶ Perfusion models.
- ▶ Optical flow constraints for joint image reconstruction and motion estimation.

About PAT:

- ▶ Emerging biomedical "hybrid" imaging technique.
- ▶ High contrast for light-absorbing structures in soft tissue.
- ▶ Non-ionizing, promising (pre-)clinical applications.
- ▶ Solve **two moderate inverse problems** instead of one severely ill-posed.
- ▶ Different sensor systems with pros and cons.
Our choice: **Fabry-Pérot interferometer**

Our Aim:

- ▶ Obtain **high spatial and temporal resolution** simultaneously.

First Results:

- ▶ Novel sensing systems are developed.
- ▶ Standard reconstruction methods fail on sub-sampled data.
- ▶ Sparse variational regularization gives promising results for sub-sampled data.
- ▶ Derivation of adjoint PAT operator enables the use of variational approaches.

Challenges:

- ▶ Realizing this potential with experimental data requires model refinement/calibration and development of pre-processing.
- ▶ Computational complexity is immense.

Outlook:

- ▶ Spatio-temporal variational models to exploit temporal redundancy.
- ▶ More suitable regularization functionals.

Thank you for
your attention!



We gratefully acknowledge the support of NVIDIA Corporation with the donation of the Tesla K40 GPU used for this research.

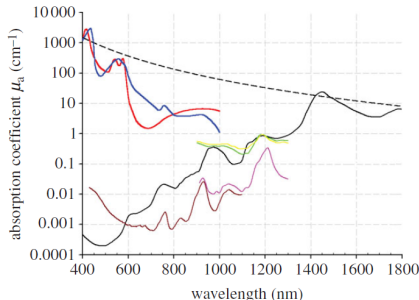
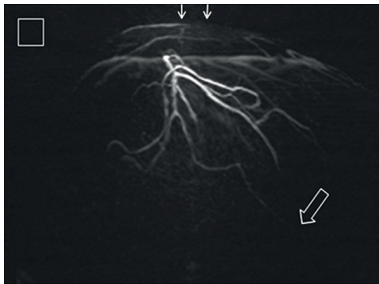
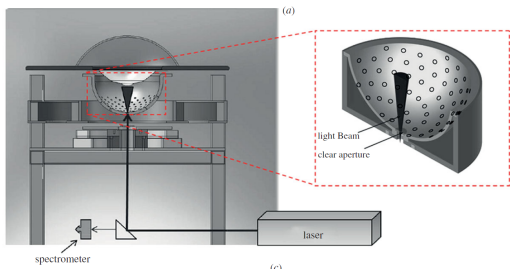


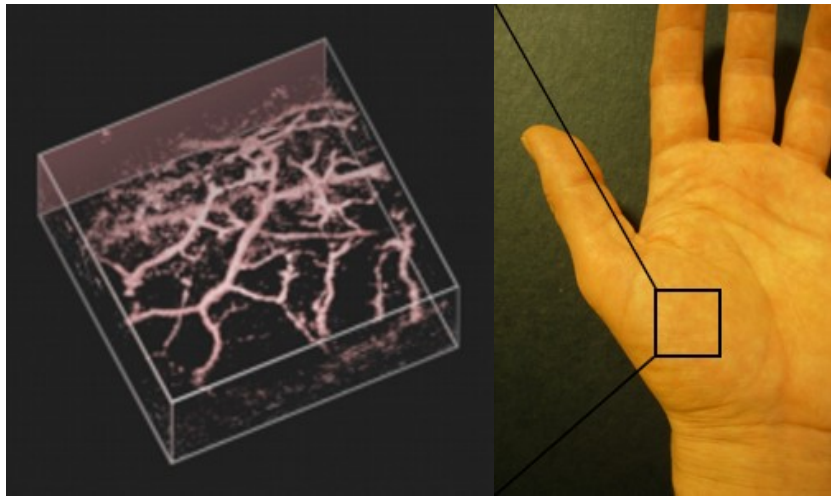
Figure 1. Absorption coefficient spectra of endogenous tissue chromophores. Oxyhaemoglobin (HbO_2), red line: (<http://omlc.ogi.edu/spectra/hemoglobin/summary.html>; 150 g l^{-1}), deoxyhaemoglobin (HHb), blue line: (<http://omlc.ogi.edu/spectra/hemoglobin/summary.html>; 150 g l^{-1}), water, black line [22] (80% by volume in tissue), lipid^(a), brown line [23] (20% by volume in tissue), lipid^(b), pink line [24], melanin, black dashed line (<http://omlc.ogi.edu/spectra/melanin/mua.html>; μ_a corresponds to that in skin). Collagen (green line) and elastin (yellow line) spectra from [24].

- ▶ High contrast between blood and water/lipid.
- ▶ Light-absorbing structures embedded in soft tissue.
- ▶ Gap between oxygenated and deoxygenated blood
~~ functional imaging.
- ▶ Different wavelengths allow quantitative spectroscopic examinations.
- ▶ Use of contrast agents for molecular imaging.

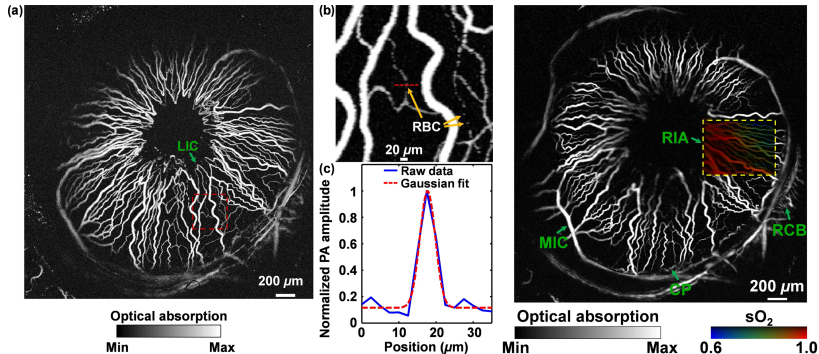
from: Paul Beard, 2011. *Biomedical photoacoustic imaging, Interface Focus*.



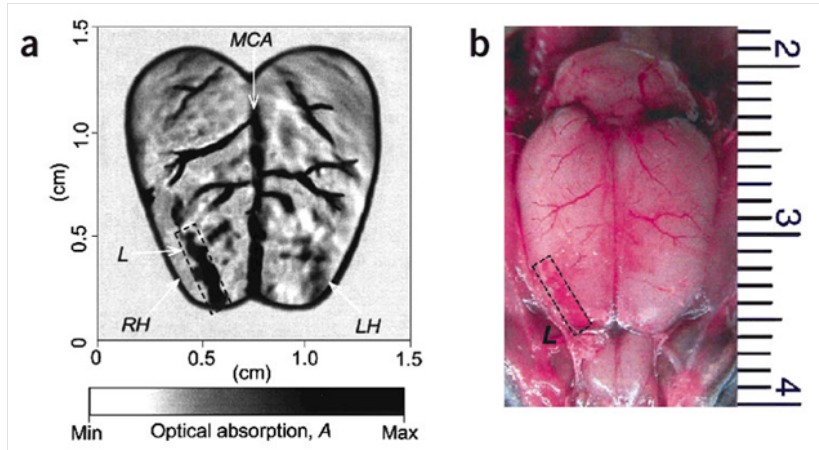
Kruger et al, 2010. *Photoacoustic angiography of the breast*, *Med. Phys.*.



taken from: <http://www.medphys.ucl.ac.uk/research/mle/images.htm>



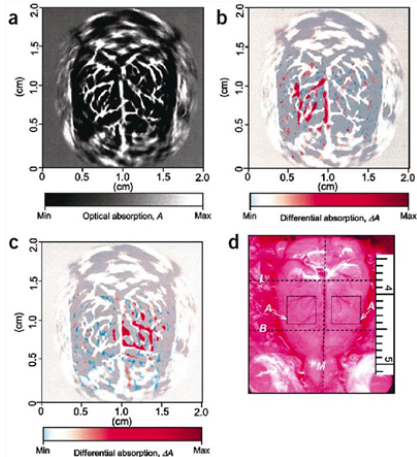
Hu et al., 2010. "Label-free photoacoustic ophthalmic angiography", *Optics Letters*



source: Wikimedia Commons

Wang et al., 2003. Non-invasive laser-induced photoacoustic tomography for structural and functional imaging of the brain *in vivo*, *Nature Biotechnology*.

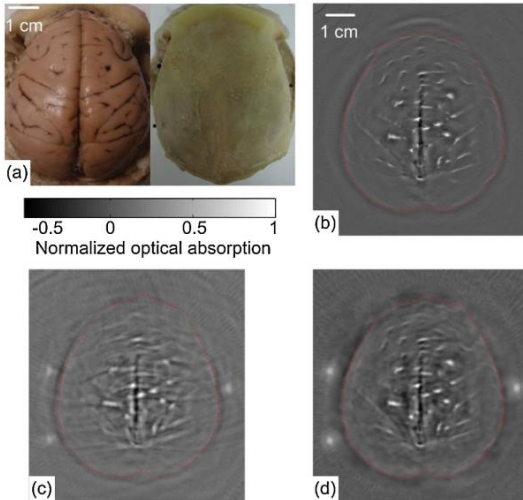
PAT Applications: Functional Brain Imaging



"Functional imaging of cerebral hemodynamic changes is response to whisker stimulation. (a) Noninvasive PAT image of the vascular pattern in the superficial layer of the rat cortex acquired with the skin and skull intact. The matrix size of the image was 1,000 (horizontal) X 1,000 (vertical), showing a 2.0 cm x 2.0 cm region. (b,c) Noninvasive functional PAT images corresponding to left-side and right-side whiskers stimulation, respectively, acquired with the skin and skull intact. These two maps of functional representations of whiskers are superimposed on the image of the vascular pattern in the superficial cortex shown in (a). (D) Open-skull photograph of the rat cortical surface. B, bregma; L, lambda; M, midline; A, activated regions corresponding to whisker stimulation (4 mm x 4 mm)."

source: Wikimedia Commons

Wang et al., 2003. *Non-invasive laser-induced photoacoustic tomography for structural and functional imaging of the brain in vivo*, *Nature Biotechnology*.



Huang et al., 2012. Aberration correction for transcranial photoacoustic tomography of primates employing adjunct image data, *J. Biomed. Opt.*